

# Morphology of Jupiter’s Polar Auroral Bright Spot Emissions via Juno-UVS Observations

Kamolporn Haewsantati<sup>1</sup>, Bertrand Bonfond<sup>2</sup>, Suwicha Wannawichian<sup>3</sup>, Randy Gladstone<sup>4</sup>, Vincent Hue<sup>4</sup>, Maarten Versteeg<sup>4</sup>, Thomas Greathouse<sup>4</sup>, Denis Grodent<sup>1</sup>, Zhonghua Yao<sup>5</sup>, William Dunn<sup>6</sup>, Jean-Claude GERARD<sup>1</sup>, Rohini Giles<sup>4</sup>, Joshua Kammer<sup>4</sup>, Ruilong Guo<sup>7</sup>, and Marissa Vogt<sup>8</sup>

<sup>1</sup>LPAP, STAR Institute, Université de Liège, Liège, Belgium

<sup>2</sup>LPAP

<sup>3</sup>Department of Physics and Materials Science

<sup>4</sup>Southwest Research Institute

<sup>5</sup>Key Laboratory of Earth and Planetary Physics, Institute of Geology and Geophysics, Chinese Academy of Sciences, Beijing, China

<sup>6</sup>Mullard Space Science Laboratory, Department of Space and Climate Physics, University College London, Dorking, UK

<sup>7</sup>Université de Liège

<sup>8</sup>Boston University

November 22, 2022

## Abstract

Since 2016, the Juno-UVS instrument has been taking spectral images of Jupiter’s auroras during its polar fly-bys. These observations provide a great opportunity to study Jupiter’s auroras in their full extent, including the nightside, which is inaccessible from Earth. We present a systematic analysis of features in Jupiter’s polar auroras called auroral bright spots observed during the first 25 Juno orbits. Bright spots were identified in 16 perijoves (PJ) out of 24 (there was no available data for perijove 2), in both the northern and southern hemispheres. The emitted power of the bright spots is time variable with peak power ranging from a few tens to a hundred of gigawatts. Moreover, we found that, for some perijoves, bright spots exhibit quasiperiodic behavior. The spots, within PJ4 and PJ16, each reappeared at almost the same system III position of their first appearance with periods of 28 and 22 minutes, respectively. This period is similar to that of quasiperiodic emissions previously identified in X-rays and various other observations. The bright spot position is in a specific region in the northern hemisphere in system III, but are scattered around the magnetic pole in the southern hemisphere, near the edge of the swirl region. Furthermore, our analysis shows that the bright spots can be seen at any local time, rather than being confined to the noon sector as previously thought based on biased observations. This suggests that the bright spots might not be firmly connected to the noon facing magnetospheric cusp processes.

# Morphology of Jupiter's Polar Auroral Bright Spot Emissions via Juno-UVS Observations

K. Haewsantati<sup>1,2,3,4</sup>, B. Bonfond<sup>1</sup>, S. Wannawichian<sup>3,4</sup>, G. R. Gladstone<sup>5</sup>, V. Hue<sup>5</sup>, M. H. Versteeg<sup>5</sup>, T. K. Greathouse<sup>5</sup>, D. Grodent<sup>1</sup>, Z. Yao<sup>6,1</sup>, W. Dunn<sup>7,8,9</sup>, J.-C. Gérard<sup>1</sup>, R. Giles<sup>5</sup>, J. Kammer<sup>5</sup>, R. Guo<sup>1</sup>, M. F. Vogt<sup>10</sup>

<sup>1</sup>LPAP, STAR Institute, Université de Liège, Liège, Belgium

<sup>2</sup>Ph.D. program in Physics, Department of Physics and Materials Science, Faculty of Science, Chiang Mai University, Chiang Mai, Thailand

<sup>3</sup>Department of Physics and Materials Science, Faculty of Science, Chiang Mai University, Chiang Mai, Thailand

<sup>4</sup>National Astronomical Research Institute of Thailand (Public Organization), Chiang Mai, Thailand

<sup>5</sup>Southwest Research Institute, San Antonio, Texas, USA

<sup>6</sup>Key Laboratory of Earth and Planetary Physics, Institute of Geology and Geophysics, Chinese Academy of Sciences, Beijing, China

<sup>7</sup>Mullard Space Science Laboratory, Department of Space and Climate Physics, University College London, Dorking, UK

<sup>8</sup>The Centre for Planetary Science at UCL/Birkbeck, London, UK

<sup>9</sup>Harvard-Smithsonian Center for Astrophysics, Smithsonian Astrophysical Observatory, Cambridge, MA USA

<sup>10</sup>Center for Space Physics, Boston University, Boston, MA, USA

## Key Points:

- Jupiter's auroral bright spots seen by Juno-UVS for the first 25 PJ mostly appear close to the edge of the polar-most region (swirl region).
- During long observation sequences (PJ4 and PJ16), bright spots recurred at approximately the same system III location every 22-28 minutes.
- The bright spots are not fixed at noon or at any specific local time, which possibly exclude the explanations involving a noon-facing cusp.

---

Corresponding author: K. Haewsantati, [K.Haewsantati@uliege.be](mailto:K.Haewsantati@uliege.be)

**Abstract**

Since 2016, the Juno-UVS instrument has been taking spectral images of Jupiter's auroras during its polar fly-bys. These observations provide a great opportunity to study Jupiter's auroras in their full extent, including the nightside, which is inaccessible from Earth. We present a systematic analysis of features in Jupiter's polar auroras called auroral bright spots observed during the first 25 Juno orbits. Bright spots were identified in 16 perijoves (PJ) out of 24 (there was no available data for perijove 2), in both the northern and southern hemispheres. The emitted power of the bright spots is time variable with peak power ranging from a few tens to a hundred of gigawatts. Moreover, we found that, for some perijoves, bright spots exhibit quasiperiodic behavior. The spots, within PJ4 and PJ16, each reappeared at almost the same system III position of their first appearance with periods of 28 and 22 minutes, respectively. This period is similar to that of quasiperiodic emissions previously identified in X-rays and various other observations. The bright spot position is in a specific region in the northern hemisphere in system III, but are scattered around the magnetic pole in the southern hemisphere, near the edge of the swirl region. Furthermore, our analysis shows that the bright spots can be seen at any local time, rather than being confined to the noon sector as previously thought based on biased observations. This suggests that the bright spots might not be firmly connected to the noon facing magnetospheric cusp processes.

**1 Introduction**

Jupiter's very bright UV auroras result from the collision between precipitating energetic particles and the atmospheric constituents in the planet's upper atmosphere. Jupiter's UV auroras are generally divided into four components: the main emissions, the equatorward emissions, the polar emissions, and the satellites' footprints. Their specific location, morphology and behavior indicates that each of them is related to specific processes in different parts of the magnetosphere. The ever-present main emissions are the easiest feature to identify. The main emissions appear as a discontinuous contour around the magnetic pole. There is a kink region in the northern hemisphere main emission contour due to a local magnetic anomaly (Grodent et al., 2008). The main emissions are driven by internal process in the middle magnetosphere at a radial distance 20-60 Jovian radii ( $R_J$ ) in the magnetosphere (Clarke et al., 2004; Vogt et al., 2011). The second component of Jupiter's aurora, the equatorward emissions, appear between the main emissions and Io's footprint and are mostly associated with magnetospheric injections (Mauk et al., 2002; Dumont et al., 2014). The multiple components of the satellite magnetic footprints are connected to the satellites of Jupiter via magnetic field lines (Bonfond, 2012). Lastly, polar auroras are characterized by the large variability of the auroral emissions in the entire region located poleward of the main emissions. The polar auroras are related to the dynamics of the outer magnetosphere, but the detailed mechanisms are still unclear. The UV polar emissions are divided into three subregions, the dark region, swirl region, and active region (Grodent et al., 2003). The dark region is characterized by its crescent shape in the dawn sector above the main emission which appears dark in ultraviolet (UV) emission (Swithenbank-Harris et al., 2019). The swirl region is a region located around the magnetic pole which consists of numerous patchy and transient features whose motion is highly variable. Despite relatively dim emissions, the swirl region usually displays spectral signatures of strong methane absorption (Bonfond, Gladstone, et al., 2017). The active region, which lies poleward from the main emission in noon to post-noon sector (Pallier & Prangé, 2001), is very dynamic. Flares, bright spots, and arc-like features are often observed in this region (Waite et al., 2001; Nichols et al., 2009; Bonfond et al., 2016).

In UV observations, one of the features of the active region studied by Pallier and Prangé (2001) is called the auroral bright spot. The bright spots that they observed in the northern hemisphere with the Hubble Space Telescope (HST) were not always ob-

80 served at the same jovi-centric system III (hereafter SIII) longitude but are typically lo-  
 81 cated close to noon magnetic local time. Pallier and Prangé (2001) therefore suggested  
 82 that this feature is the signature of the polar cusp process. Another feature, polar flares,  
 83 reported by Waite et al. (2001), were identified as short-lived but intense features in the  
 84 active region that can suddenly brighten within a short time scale (10s of seconds). The  
 85 flares occurring in the southern hemisphere were reported to reappear periodically with  
 86 time intervals of 2-3 minutes (Bonfond et al., 2011). They were mapped to the dayside  
 87 in the outer magnetosphere by using the magnetic mapping model developed by Vogt  
 88 et al. (2011, 2015). Bonfond et al. (2016) revisited this study and found the quasiperi-  
 89 odic (QP) flares among half of their augmented dataset. These features appeared in both  
 90 northern and southern hemispheres, and some of them appeared to brighten in phase.  
 91 From their location, size and behaviors, the flares appear to correspond to closed field  
 92 lines mapping to the dayside outer magnetosphere. Besides, the QP emissions also oc-  
 93 cur in the main emission region. Nichols, Yeoman, et al. (2017) revealed a  $\sim 10$  min pe-  
 94 riod pulsating aurora feature in the main emission, which has the same period as the Alfvén  
 95 wave travel time between the equatorial sheet and the ionosphere.

96 Quasi-periodic pulsations had been reported and studied across a wide range of datasets  
 97 in the Jovian magnetosphere. For example, McKibben et al. (1993) identified 40-minute  
 98 periodicity in electron bursts observed by Ulysses, with a few cases showing shorter pe-  
 99 riods (2-3 minutes). Similarly, MacDowall et al. (1993) reported two classes of QP ra-  
 100 dio bursts with periods of 15 and 40 minutes, respectively. There was also a report by  
 101 Pryor et al. (2005) of the correspondence of 2 minutes long QP flares observed by Cassini  
 102 Ultraviolet Imaging Spectrograph (UVIS) and low frequency radio bursts observed by  
 103 Cassini Radio and Plasma Wave Spectrometer (RPWS) and Galileo Plasma Wave Spec-  
 104 trometer (PWS). Furthermore, many QP pulsations are reported from the analysis of  
 105 X-ray observations with periods in range 10-100 minutes (Gladstone et al., 2002; Elsner  
 106 et al., 2005; Dunn et al., 2016, 2017, 2020; Jackman et al., 2018; Weigt et al., 2020; Wibisono  
 107 et al., 2020). Gladstone et al. (2002) presented the pulsation emissions from hot spot re-  
 108 gion in the northern hemisphere with 45 minutes period. Elsner et al. (2005) showed the  
 109 relation between X-ray pulsations with  $\sim 40$  minutes period with Ulysses radio observa-  
 110 tion. Bunce et al. (2004) suggested that pulsed reconnection on the dayside magnetopause  
 111 could be the source of the pulsations in both the X-ray and UV auroras.

112 In summary, the QP emissions in the active region typically found in HST obser-  
 113 vations of the UV auroras have shorter periods (2-3 minutes) than X-ray and radio QP  
 114 emissions (10s of minutes). However, the maximum length for a continual observation  
 115 obtain from HST is about 45 minutes which limits the longest periodicity it can detect  
 116 to about 20 minutes. HST observations cannot explore the night side of the aurora and  
 117 are biased toward configurations in which the magnetic pole is tilted towards the Earth.  
 118 In contrast, observations from Juno allow for a complete view of the auroras, including  
 119 the nightside, as well as longer time interval observations up to a few consecutive hours.  
 120 Here, we present a systematic study of the bright spots observed with the ultraviolet spec-  
 121 trograph on board Juno (Juno-UVS) during the first 25 orbits, with a particular focus  
 122 on bright spots location (Section 3.1) and their variability (Section 3.2).

## 123 2 Juno-UVS observations and processing methods

124 The Juno-UVS instrument is a UV photon-counting imaging spectrograph oper-  
 125 ating in the 68 to 210 nm wavelength range. There is a flat scan mirror at the entrance  
 126 of the instrument, which allows it to look at targets up to  $\pm 30^\circ$  away from the Juno spin  
 127 plane. Its “dog bone” shaped slit consists of three contiguous segments with fields-of-  
 128 view (FOV) of  $0.2^\circ \times 2.5^\circ$ ,  $0.025^\circ \times 2^\circ$ , and  $0.2^\circ \times 2.5^\circ$ . The data obtained from UVS  
 129 consist of a list of photon detection events with X position of the photon count on the  
 130 detector corresponding to the spectral dimension and the Y position of the spatial di-  
 131 mension along the slit (Gladstone et al., 2017; Greathouse et al., 2013; Hue et al., 2019).

132 The spacecraft spins every  $\sim 30$  seconds. Every spin, a spectrally resolved image can be  
 133 reconstructed based on the motion of the field of view across the planet. The pointing  
 134 mirror can target a different region of the aurora at each spin. The polar projected im-  
 135 ages used for this study assume that the aurora originates from a mean altitude of 400  
 136 km above 1 bar level (Bonfond et al., 2015). For further analysis, the photon counts are  
 137 converted to brightness in kilo-Rayleighs (kR) which corresponds to the total unabsorbed  
 138  $\text{H}_2$  Lyman emissions and Werner bands. The conversion can be done by multiplying the  
 139 intensity obtained in the 155-162 nm spectral range with a conversion factor of 8.1, us-  
 140 ing to the  $\text{H}_2$  synthetic spectrum calculated by Gustin et al. (2013). Then, the emitted  
 141 power can be computed by multiplying the brightness with the surface area and with  
 142 the mean energy of a UV photon. Uncertainty on the brightness calculation mainly comes  
 143 from the in-flight calibration of the instrument effective area (Hue et al., 2019). In com-  
 144 parison, the uncertainty related to the shot noise is negligible here because we integrate  
 145 over a relatively large region of the aurora (Gérard et al., 2019).

146 The bright spot feature is characterized as a distinct feature with a compact shape,  
 147 which is very bright (typically more than 10 times brighter) in comparison to the sur-  
 148 rounding area in polar region. In order to identify the area of the bright spot, we first  
 149 remove a mean background emission and then we consider the region whose brightness  
 150 is above twice the standard deviation of surrounding area's brightness. We then fit the  
 151 shape of bright spot with an ellipse and we compute the emitted power in this ellipse.  
 152 In this case, the main source of uncertainty lies in the selection of the area of interest.  
 153 Hence, the uncertainty is calculated by assuming an elliptical reference area 25% smaller  
 154 and then 25% larger than the best fit ellipse. To assess the evolution of the total power  
 155 in the region of interest, the ellipse area is fitted based only on the images for which the  
 156 bright spot can be clearly identified. Then, for a given dataset (i.e. a specific spot dur-  
 157 ing a given perijove), the union of the fitted ellipses is used as a reference surface to com-  
 158 pute the total power, so that the area of interest remains the same during the whole se-  
 159 quence.

### 160 3 Results

161 From UVS data obtained during the first 25 perijoves (PJ), the bright spots ap-  
 162 pear in both northern and southern hemispheres (Figure 1). Northern hemisphere bright  
 163 spots have been identified in PJ1, PJ3, PJ6, PJ8, and PJ13. However, in our dataset,  
 164 the bright spots appear more often in the southern aurora, which can be seen in PJ4,  
 165 PJ8, PJ9, PJ12, PJ14, PJ15, PJ16, and PJ20-PJ24. Indeed, as Juno's orbit precesses  
 166 and as Juno's apojoive moves from dawn to midnight, the time interval available for ob-  
 167 servations of the northern hemisphere decreased as the mission goes. It should be noted  
 168 that two bright spots which appear in the same perijove at different positions are ob-  
 169 served in PJ3, PJ12, PJ21, and PJ23. The bright spots sometimes appear as compact  
 170 small spots, with smallest surface area  $3.5 \times 10^5 \text{ km}^2$ , and sometimes it covers a larger  
 171 area ( $2.07 \times 10^7 \text{ km}^2$ ). The total power emission usually lies in the range of tens of gi-  
 172 gawatts (GW), but some spots' power can occasionally rise up to a hundred GW (e.g.  
 173 PJ16 at 01:52:04, cf. Figure 6). The summary of bright spots area, power, magnetic flux  
 174 corresponding to the spot's area, and the local time in Jupiter's ionosphere are shown  
 175 in Figure 2. In the next subsections, we will discuss the variability of the bright spots'  
 176 power and position. As we will see, the bright spots usually reappear at almost the same  
 177 position in SIII coordinates. Moreover, the time intervals between the occurrence of con-  
 178 secutive spots in a given perijove range from a few minutes to more than half an hour.

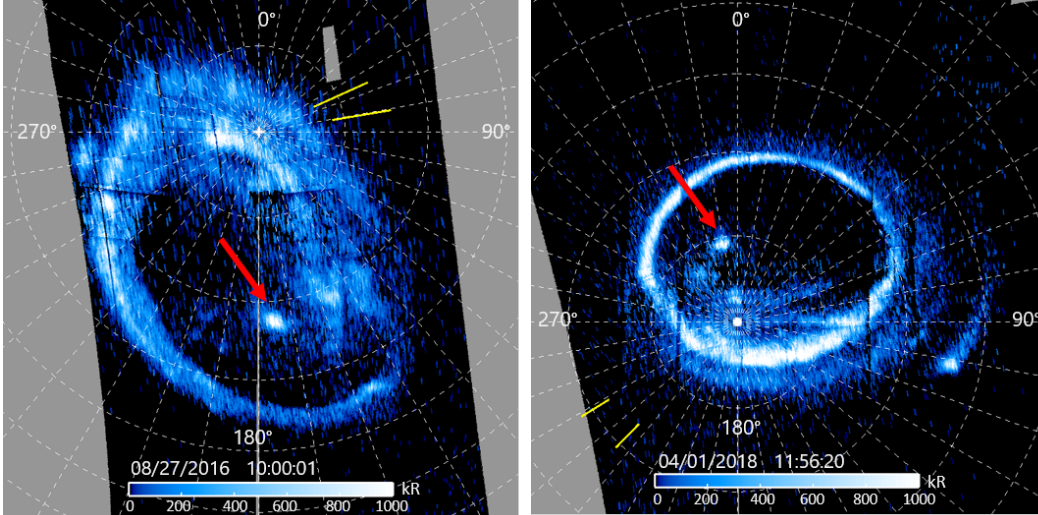


**Figure 1.** Two examples of bright spot in Jupiter’s polar auroras (indicated by red arrows) as observed by Juno-UVS in the northern hemisphere during PJ1 (left) and the southern hemisphere during PJ12 (right). The grid represents meridians and parallels in the SIII, spaced every  $10^\circ$ . Each polar projection is a combination of observations acquired during several spins in order to create a full view of Jupiter’s aurora. Two short-yellow lines show the subsolar longitudes of the start time and stop time of combined data.

179

### 3.1 Location and Local Time

180

#### 3.1.1 Position in System III

181

182

183

184

185

186

187

188

189

190

The pixel positions of the peak of bright spots were used to calculate the latitudinal and longitudinal coordinates of spot features in the ionosphere. The bright spots in the northern hemisphere are mostly clustered in a restricted region. As shown in Figure 3, the positions of bright spots, except for PJ8 data (marked as green cross), are in range of 60-70 degrees latitude and 160-190 SIII degrees longitude. Incidentally, this region is also the X-ray hot spot regions (Gladstone et al., 2002; Dunn et al., 2016, 2017; Weigt et al., 2020; Dunn et al., 2020). One notable exception is found during PJ8, during which the bright spot is at  $\sim 82$  degrees latitude and 216.5 degrees SIII longitude. On the other hand, the bright spots detected in the southern hemisphere scatter around the magnetic pole.

191

192

193

194

195

196

197

198

199

Figure 3 shows the positions of the bright spots in SIII, superimposed on the surface magnetic field strength from the JRM09 model (Connerney et al., 2018). Considering the two hemispheres together, it appears that the bright spots favour areas where the surface magnetic field is larger than  $8 \times 10^5$  nT. The only exception being the bright spots observed in the north during PJ8, which is one of the dimmest of our selection. Moreover, we calculated for the solar zenith angle at the bright spots positions (see supporting information). The bright spots occur even when the sun is at high zenith angle or even below the horizon. Therefore, the bright spots might be independence on the conductivity of the ionosphere.

200

#### 3.1.2 Position with respect to the swirl region

201

202

We also plot the bright spot positions over maps of the color ratio, in order to locate them with respect to the swirl region. These are produced from the ratio between

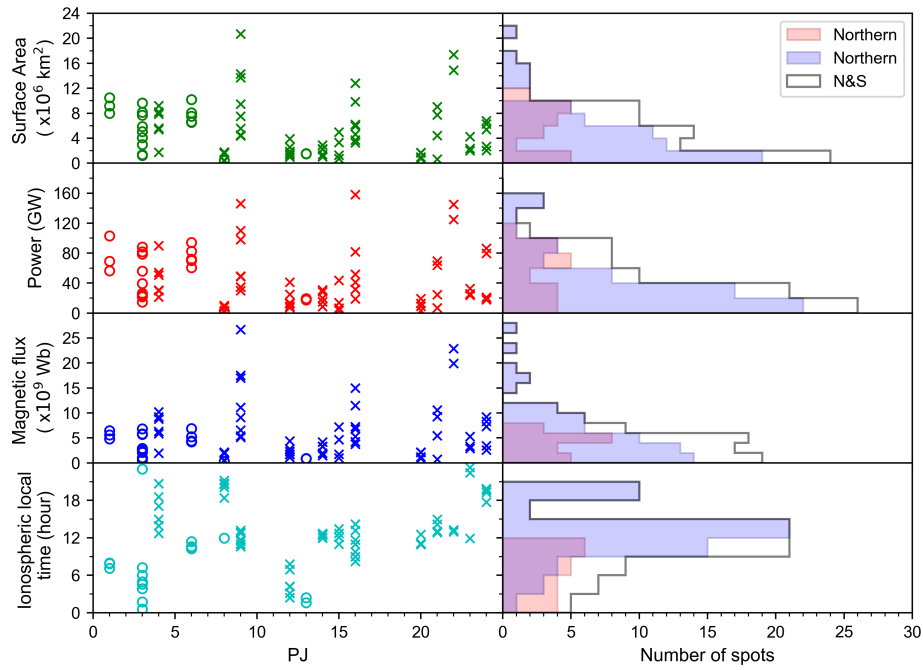


**Figure 2.** Top three panels are distribution of the surface area, the power emission, and the magnetic flux inside bright spot's area based on elliptical fit. Bottom panel shows ionospheric local time of bright spot's peak emission. On the left panels, those values vary at different PJs, for the northern spots (circles) and the southern spots (crosses). The total numbers of spots for each parameter from each hemisphere are presented by histogram on the right panels.

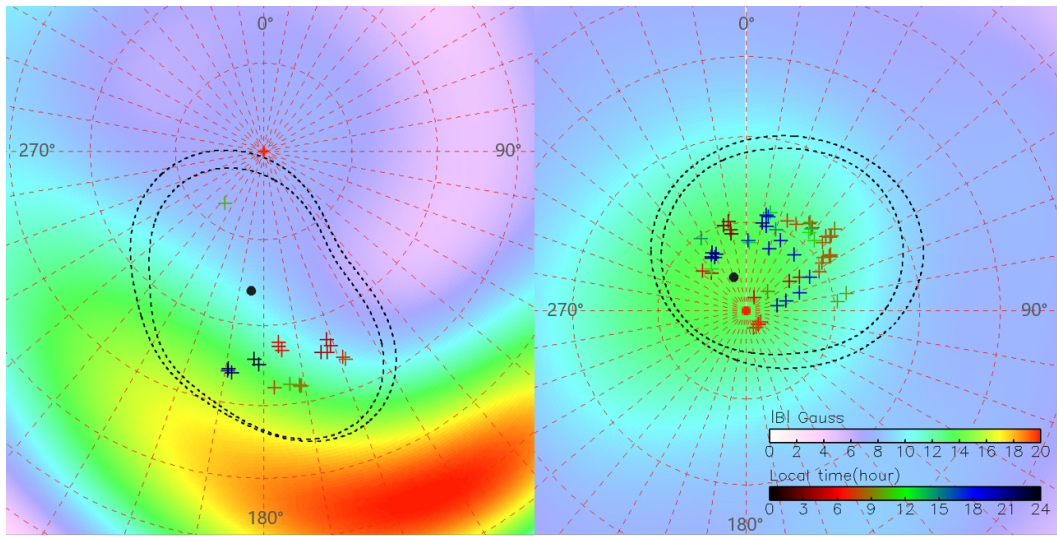


**Figure 3.** Polar projections with the same coordinates as Figure 1, show the magnetic field magnitude (in Gauss) on the surface of Jupiter based on JRM09 model (Connerney et al., 2018) and positions of bright spots observed in Jupiter’s polar region for (left) northern and (right) southern hemispheres. The two dash contours are the statistical locations of the main emission for the compressed (inner contour) and expanded (outer contour) cases observed by HST in 2007 (Bonfond et al., 2012). The black dot indicates the magnetic pole of each hemisphere (Bonfond, Saur, et al., 2017; Connerney et al., 2018). The colors of bright spot positions correspond to their local times, acquired by magnetic mapping model developed by Vogt et al. (2011, 2015) couple with JRM09 model.

emission intensity of molecular hydrogen at two wavelength ranges, one unaffected by methane absorption (1550-1620 Å) and one affected by methane absorption (1250-1300 Å). On these maps, the swirl region displays distinctive strong absorption signatures (Bonfond, Gladstone, et al., 2017). Figure 4 shows examples of such color ratio maps from PJ6 (north, left) and PJ16 (south, right) with the position of the bright spots identified during these perijoves over-plotted. The results show that the most bright spots are located near the boundary of the high color ratio regions (swirl region). The most diverse position took place during PJ1, for which the bright spots are located inside the high color ratio region instead of at its boundary (see supporting information).

### 3.1.3 Position in magnetic local time

Observations carried out with HST suggested that the bright spot are located in the magnetic noon sector (Pallier & Prangé, 2001). However, HST observations are biased in favor of a configuration when the magnetic pole faces the Earth and the night side of the aurora is out of sight. On the contrary, Juno-UVS allows us to get an unbiased understanding of the mapping of the bright spots in the magnetosphere. We applied the magnetosphere-ionosphere mapping flux equivalence method of Vogt et al. (2011, 2015) couple with the JRM09 internal magnetic field model (Connerney et al., 2018) to evaluate the magnetospheric source location in the outer magnetosphere. It should be noted however that such a model is increasingly inaccurate as one moves from Ganymede's footprint path towards the pole. The bright spots are generally mapping to positions beyond 150  $R_J$  or beyond the dayside magnetopause, which means the positions are beyond the model's limit. In order to estimate the result despite these limitations, we extrapolate the spots' position radially until we obtain a predicted position from the model. This can be done by tracing a line on the polar plot, from the magnetic pole toward the bright spot's position and keep moving equatorward until we obtain the latitude and longitude that can be mapped to a position inside the model boundary. In the southern hemisphere, we chose the point where the JRM09 magnetic field is vertical as the southern magnetic pole, at approximately -86 degrees latitude and 340 degrees SIII longitude. In the northern hemisphere, the magnetic field is so complex that there is no point where the field is vertical in the auroral polar region. Hence, we chose the barycenter of the aurora as defined in Bonfond, Saur, et al. (2017), at 74 degrees latitude and 185 degrees SIII longitude. The polar projection maps of bright spots and the corresponding magnetic local time are shown by the color of the crosses in Figure 3. The local times of the bright spots in the northern hemisphere range from late evening through midnight to late morning while the local times for bright spot in the southern hemisphere spread in entire range. Finally, the bottom panel of Figure 2 shows the distribution of the ionospheric local time, considering the magnetic pole defined above as the center and the Sun direction as noon. The distribution of ionospheric local times of bright spots is similar to the distribution of magnetic local times. This wide distribution of local times significantly contrasts with previous studies which suggested that the bright spot could correspond to noon local time facing magnetospheric cusp.

### 3.1.4 Bright spot's motion with time

As the appearance of the bright spots are detected, the cylindrical map of Figure 5 shows the track change in bright spot's latitude and SIII longitude. Please note that this figure shows both the northern and southern spots in the same plot which are separated by different colors. In most cases, the positions of the northern and southern spots only change slightly in both latitude and longitude (a few thousand kilometers). The exception spots whose locations vary noticeably are the northern spot from PJ3 and the southern spots from PJ9, PJ16 and PJ24. The motions of the bright spots at latitudes beyond  $\pm 85$  degrees, i.e. PJ14 and PJ15, are actually very small because the positions lie close to the rotational pole. The bright spot found in PJ3(N), deep blue symbol in

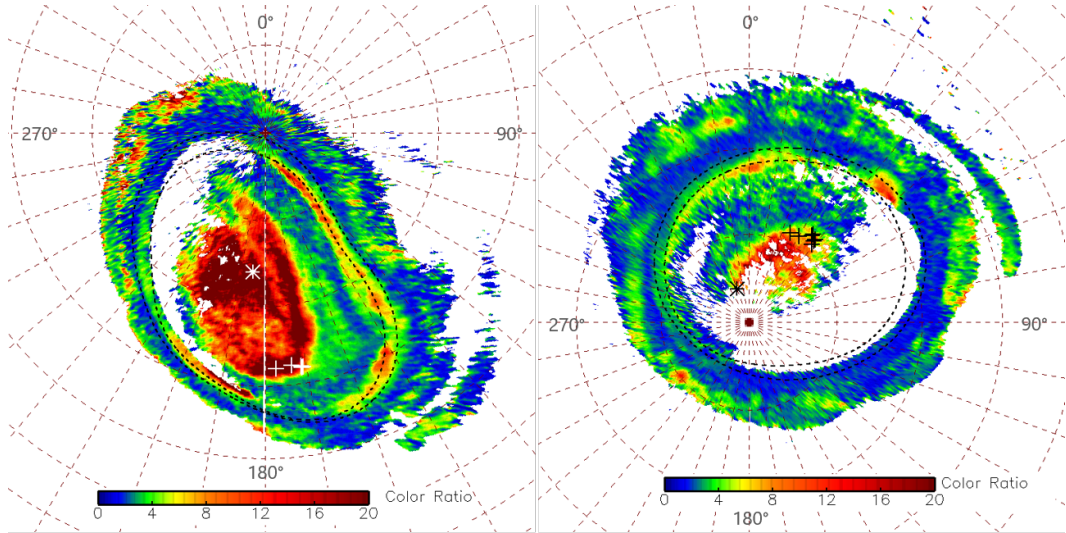


**Figure 4.** The bright spots positions and the color ratio map observed from (left) PJ6 and (right) PJ16. The coordinates and two dashed contours are described in Figure 1. The plus signs are the bright spots observed in (left) PJ6 and (right) PJ16. The asterisk signs represent the magnetic poles, for (left) north and (right) south hemispheres (Bonfond, Saur, et al., 2017; Connerney et al., 2018).

254 Figure 5, shows the variation in position starting from 164 to 158 SIII degrees longitude  
 255 and 3 degrees shifted in latitude. For the bright spot in the southern hemisphere, the  
 256 bright spot from PJ9 appears to move from low to high latitude starting from -76 to -  
 257 80 degrees and from 47 to 62 degrees in SIII longitude while a bright spot from PJ24 con-  
 258 tinuously change position from 20 to 70 degrees longitude. These results show that the  
 259 bright spots are mostly fixed in specific positions as Jupiter rotates, while, in a few cases,  
 260 their positions changed. The rates of change in positions are also not related to Jupiter's  
 261 rotation period. Moreover, the motions do not have any systematic pattern since we found  
 262 cases where the SIII longitude increased or decreased over time.

### 263 3.2 The bright spot's power variations

264 Since the bright spot reappears at nearly the same position, we consider the emis-  
 265 sions in the same region to be part of a continuous sequence. For a given perijove, the  
 266 bright spots brighten and fade with a time interval on the order of minutes. When we  
 267 consider the whole available dataset, this time interval is in the 3-47 minutes range.

268 Unfortunately, the continuous tracking of the bright spot emitted power is com-  
 269 plicated by the fact that the field of view of the instrument varies significantly with time,  
 270 which leads to discontinuous sampling rate, or inappropriately short sequences, to in-  
 271 vestigate periodicities. Moreover, as the mission progressed, the duration of the obser-  
 272 vations in the northern hemisphere decreased from a few hours to a few tens of minutes.  
 273 Fortunately, two particular cases, from PJ4 and PJ16 in the South, allowed for a quasi-  
 274 continuous monitoring of the bright spots' power variations for 3 to 4 hours.

275 Figure 6 shows the power variation as a function of time for one particular south-  
 276 ern bright spot during PJ16 (a similar plot for PJ4 can be found in the supplemental  
 277 material). The shaded areas indicate time intervals during which UVS field of view missed  
 278 more than 50% of the region of interest defined by the union of the fitted ellipses. The

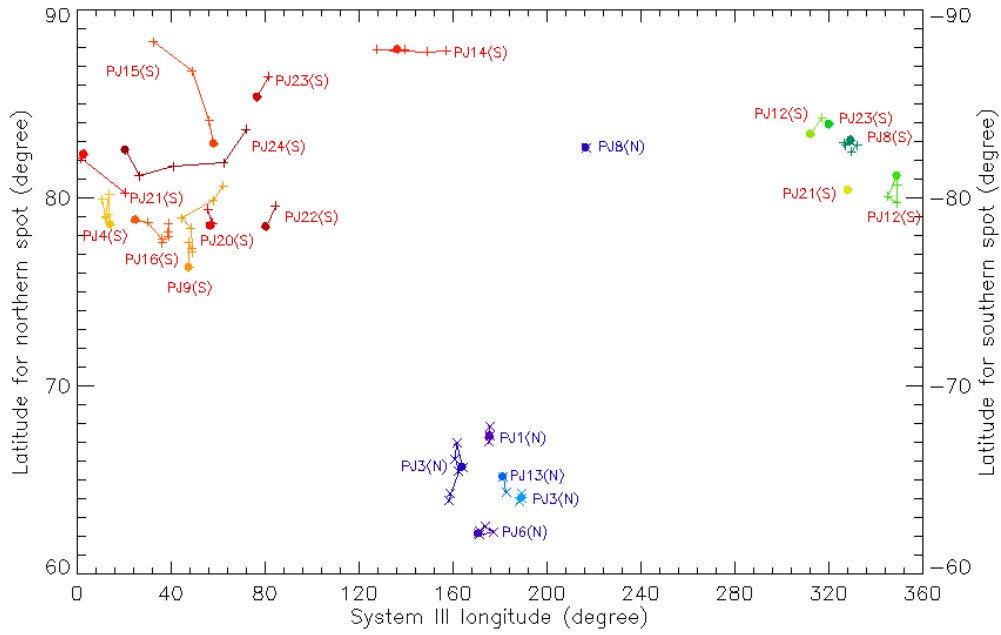


**Figure 5.** Latitude and SIII longitude map shows the positions of bright spot observed in northern hemisphere (plus sign) and southern hemisphere (cross sign). Each line is named by the perijove number and the hemisphere, e.g. PJ1(N) is for northern bright spot from PJ1. The northern spots are colored in shades of blue and southern spots use a color gradient from green to red. The line connecting each data presents the motion of bright spot with observing time order. The large dot for each line represents the first position of the bright spot during a sequence.

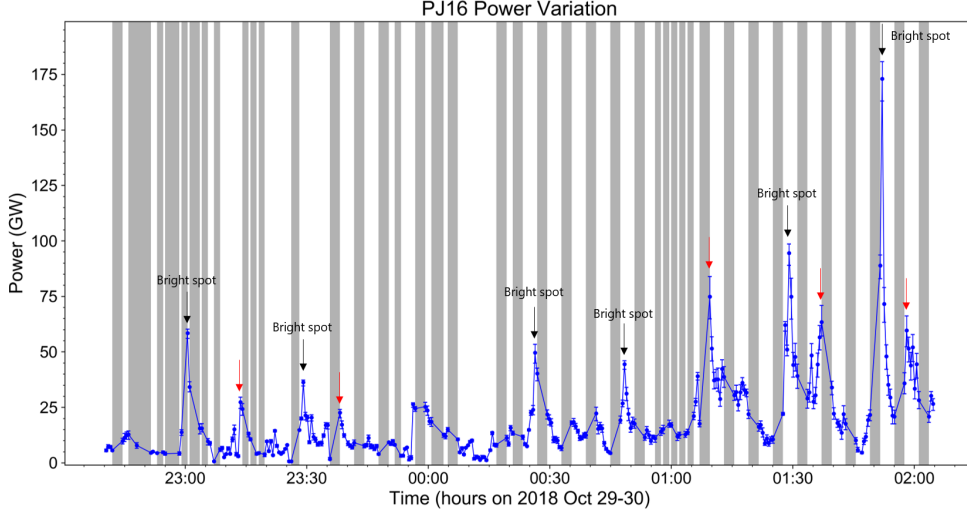


**Figure 6.** The time variation of power emission observed in PJ16 from 22:40:00 UT on 29 Oct 2018 to 02:00:00 UT on 30 Oct 2018. The gray boxes illustrate the times that the bright spot region was not covered by the UVS field of view. Black arrows indicate the times when clear bright spots are detected while red arrows show the additional peaks at which no bright spot appears in the region of interest.

279 power peaks of the bright spot are above 35 GW and can reach up to 170 GW. More-  
 280 over, a clear repetitive pattern is identified in the time series. In addition to the well-  
 281 identified bright spots (black arrow), the plot shows that there are additional power peaks  
 282 (indicated by red arrows) that correspond to more diffuse features that were not ident-  
 283 tified as bright spots at first. Nevertheless, these power peaks are close to shaded areas,  
 284 suggesting that UVS might have missed the time interval during which a clear bright spot  
 285 could have been identified. The time intervals between consecutive peaks in this plot ranges  
 286 from 5 to 42 minutes, with a typical interval around 25 minutes. In order to get quan-  
 287 titative results, we also determine the spot's reappearance period with a Lomb-Scargle  
 288 analysis (see supporting information). The results confirm that the bright spot emissions  
 289 PJ16 repeatedly brighten with period of 23 min. Similarly, results from PJ4 show a  $\sim$   
 290 28-minute period. We note that these periods are similar to earlier reports about Jupiter's  
 291 quasiperiodic phenomena (MacDowall et al., 1993; McKibben et al., 1993; Dunn et al.,  
 292 2016; Jackman et al., 2018; Wibisono et al., 2020).

#### 293 4 Discussions and Conclusions

294 Following the interpretation of Pallier and Prangé (2001), we expected that the bright  
 295 spots would appear near noon magnetic local time and may correspond to the Jovian  
 296 magnetospheric cusp. Instead, our results show that the bright spots can be seen in var-  
 297 ious ionospheric local times and are observed at positions mapping to a wide range of  
 298 magnetic local times in the distant magnetosphere. Moreover, several bright spots were  
 299 observed at different locations during the same observational sequence. We show that  
 300 the bright spots mostly lie near the edge of the swirl region (with one exception during  
 301 PJ1). Furthermore, we show that the bright spots often re-appear at the same SIII po-  
 302 sition during a given sequence, suggesting that the source region (wherever it is along  
 303 the field line) corotates with Jupiter. Moreover, with additional results regarding the lo-  
 304 cal time, these observations thus rule out a simple interpretation according to which the

bright spot is a direct counterpart of a noon-facing magnetospheric cusp. However, Zhang et al. (2020) suggested that topology of the polar-most field lines could be very complex and helical, leading to atypical definition of a magnetospheric cusp for Jupiter and an unclear mapping of the field lines. Thus, we cannot confirm nor rule out that the bright spot could be related to some complex Jovian cusp processes.

Finally, our study of the variations of the emitted power shows that the bright spots are not sporadic random events, since they reoccur at nearly the same position after some typical time interval from a few minutes to a few tens of minutes. The bright spot emissions observed during PJ4 and PJ16 are particularly interesting because of the length of the observed sequence, and quasi-periodicities of 22-28 minutes are detected. Such timescales are hard to identify with the limited duration of HST observations ( $\sim 45$  minutes). Even if we do not exclude a possible relationship between the bright spots and the flares, it should be noted that the periodicities identified here for the bright spots are one order of magnitude longer ( $\sim 30$  minutes) than the one identified for the 2-3 minutes QP flares (Bonfond et al., 2011, 2016; Nichols, Badman, et al., 2017). Moreover, while most of the bright spots appear close to the boundary of the swirl region, the flares rather take place on the noon and dusk sides of the active region (Bonfond et al., 2016; Nichols, Badman, et al., 2017). Instead, the reappearances of bright spots several times during the same day suggest a link with other quasi-periodic behavior with similar time scales. It should be noted that the 3-47 minutes time intervals between consecutive emissions are also the same range as quasi-periodic pulsations identified in radio emissions (MacDowall et al., 1993), relativistic electrons (McKibben et al., 1993), Alfvén waves (Manners et al., 2018) and X-ray pulsations (Jackman et al., 2018; Wibisono et al., 2020). Further studies of the connection between these different phenomena will certainly provide important information concerning the processes giving rise to these emissions.

### Acknowledgments

K. H. would like to grateful thank for financial support from Science Achievement Scholarship of Thailand (SAST) and Ph.D. program in Physics, Chiang Mai university. K. H. and S. W. are supported by National Astronomical Research Institute of Thailand (NARIT). B. B. is a Research Associate of the Fonds de la Recherche Scientifique - FNRS. B. B., D. G., Z. Y. and J.-C. G. acknowledge the support from the PRODEX Programme of European Space Agency (ESA). G. R. G., V. H., M. H. V., and T. K. G., are funded by the Southwest Research Institute. W. Dunn is supported by STFC research grant to UCL and SAO fellowship to Harvard-Smithsonian Centre for Astrophysics and by ESA. The data included herein are archived in NASA's Planetary Data System ([http://pds-atmospheres.nmsu.edu/data\\_and\\_services/atmospheres\\_data/JUNO/juno.html](http://pds-atmospheres.nmsu.edu/data_and_services/atmospheres_data/JUNO/juno.html)). This research was partly supported by NARIT. Additional support was from Thailand Research Fund grants RTA6280002. We are grateful to NASA and contributing institutions which have made the Juno mission possible. This work was funded by NASA's New Frontiers Program for Juno via contract with the Southwest Research Institute.

### References

- Bonfond, B. (2012). When Moons Create Aurora: The Satellite Footprints on Giant Planets. In *Geophysical Monograph Series*. AGU. Retrieved 2020-07-08, from <https://orbi.uliege.be/handle/2268/136072> doi: 10.1029/2011GM001169
- Bonfond, B., Gladstone, G. R., Grodent, D., Greathouse, T. K., Versteeg, M. H., Hue, V., ... Kurth, W. S. (2017, May). Morphology of the UV auroresae Jupiter during Juno's first perijove observations. *Geophysical Research Letters*, *44*(10), 4463–4471. Retrieved 2019-02-25, from <https://agupubs.onlinelibrary.wiley.com/doi/full/10.1002/2017GL073114> doi: 10.1002/2017GL073114

- 356 Bonfond, B., Grodent, D., Badman, S. V., Gérard, J.-C., & Radioti, A. (2016,  
357 December). Dynamics of the flares in the active polar region of Jupiter.  
358 *Geophysical Research Letters*, *43*(23), 11,963–11,970. Retrieved 2018-08-  
359 31, from [https://agupubs.onlinelibrary.wiley.com/doi/abs/10.1002/  
360 2016GL071757](https://agupubs.onlinelibrary.wiley.com/doi/abs/10.1002/2016GL071757) doi: 10.1002/2016GL071757
- 361 Bonfond, B., Grodent, D., Gérard, J.-C., Stallard, T., Clarke, J. T., Yoneda, M.,  
362 ... Gustin, J. (2012, January). Auroral evidence of Io's control over the  
363 magnetosphere of Jupiter. *Geophysical Research Letters*, *39*(1). Retrieved  
364 2018-08-31, from [https://agupubs.onlinelibrary.wiley.com/doi/abs/  
365 10.1029/2011GL050253](https://agupubs.onlinelibrary.wiley.com/doi/abs/10.1029/2011GL050253) doi: 10.1029/2011GL050253
- 366 Bonfond, B., Gustin, J., Gérard, J.-C., Grodent, D., Radioti, A., Palmaerts, B.,  
367 ... Tao, C. (2015, October). The far-ultraviolet main auroral emission at  
368 Jupiter – Part 2: Vertical emission profile. *Ann. Geophys.*, *33*(10), 1211–1219.  
369 Retrieved 2018-08-31, from [https://www.ann-geophys.net/33/1211/2015/  
370 doi: 10.5194/angeo-33-1211-2015](https://www.ann-geophys.net/33/1211/2015/)
- 371 Bonfond, B., Saur, J., Grodent, D., Badman, S. V., Bisikalo, D., Shematovich, V.,  
372 ... Radioti, A. (2017, August). The tails of the satellite auroral footprints at  
373 Jupiter. *Journal of Geophysical Research: Space Physics*, *122*(8), 7985–7996.  
374 Retrieved 2018-08-31, from [https://agupubs.onlinelibrary.wiley.com/  
375 doi/abs/10.1002/2017JA024370](https://agupubs.onlinelibrary.wiley.com/doi/abs/10.1002/2017JA024370) doi: 10.1002/2017JA024370
- 376 Bonfond, B., Vogt, M. F., Gérard, J.-C., Grodent, D., Radioti, A., & Coumans, V.  
377 (2011, January). Quasi-periodic polar flares at Jupiter: A signature of pulsed  
378 dayside reconnections? *Geophysical Research Letters*, *38*(2). Retrieved 2018-  
379 08-31, from [https://agupubs.onlinelibrary.wiley.com/doi/abs/10.1029/  
380 2010GL045981](https://agupubs.onlinelibrary.wiley.com/doi/abs/10.1029/2010GL045981) doi: 10.1029/2010GL045981
- 381 Bunce, E. J., Cowley, S. W. H., & Yeoman, T. K. (2004, September). Jovian  
382 cusp processes: Implications for the polar aurora. *Journal of Geophysical  
383 Research: Space Physics*, *109*(A9). Retrieved 2018-08-31, from [https://  
384 agupubs.onlinelibrary.wiley.com/doi/abs/10.1029/2003JA010280](https://agupubs.onlinelibrary.wiley.com/doi/abs/10.1029/2003JA010280) doi:  
385 10.1029/2003JA010280
- 386 Clarke, J. T., Grodent, D., Cowley, S. W. H., Bunce, E. J., Zarka, P., Connerney,  
387 J. E. P., & Satoh, T. (2004). Jupiter's aurora. In (pp. 639–670). *Jupiter. The  
388 Planet, Satellites and Magnetosphere.*
- 389 Connerney, J. E. P., Kotsiaros, S., Oliverson, R. J., Espley, J. R., Joergensen,  
390 J. L., Joergensen, P. S., ... Levin, S. M. (2018, March). A New Model  
391 of Jupiter's Magnetic Field From Juno's First Nine Orbits. *Geophysical  
392 Research Letters*, *45*(6), 2590–2596. Retrieved 2018-10-25, from [https://  
393 agupubs.onlinelibrary.wiley.com/doi/abs/10.1002/2018GL077312](https://agupubs.onlinelibrary.wiley.com/doi/abs/10.1002/2018GL077312) doi:  
394 10.1002/2018GL077312
- 395 Dumont, M., Grodent, D., Radioti, A., Bonfond, B., & Gérard, J.-C. (2014, Decem-  
396 ber). Jupiter's equatorward auroral features: Possible signatures of magneto-  
397 spheric injections. *Journal of Geophysical Research: Space Physics*, *119*(12),  
398 10,068–10,077. Retrieved 2018-09-03, from [https://agupubs.onlinelibrary  
399 .wiley.com/doi/abs/10.1002/2014JA020527](https://agupubs.onlinelibrary.wiley.com/doi/abs/10.1002/2014JA020527) doi: 10.1002/2014JA020527
- 400 Dunn, W. R., Branduardi-Raymont, G., Ray, L. C., Jackman, C. M., Kraft, R. P.,  
401 Elsner, R. F., ... Coates, A. J. (2017, November). The independent pulsations  
402 of Jupiter's northern and southern X-ray auroras. *Nature Astronomy*, *1*(11),  
403 758–764. Retrieved 2020-03-23, from [https://www.nature.com/articles/  
404 s41550-017-0262-6](https://www.nature.com/articles/s41550-017-0262-6) (Number: 11 Publisher: Nature Publishing Group) doi:  
405 10.1038/s41550-017-0262-6
- 406 Dunn, W. R., Branduardi-Raymont, G., Elsner, R. F., Vogt, M. F., Lamy,  
407 L., Ford, P. G., ... Jasinski, J. M. (2016). The impact of an ICME  
408 on the Jovian X-ray aurora. *Journal of Geophysical Research: Space  
409 Physics*, *121*(3), 2274–2307. Retrieved 2020-03-23, from [https://agupubs  
410 .onlinelibrary.wiley.com/doi/abs/10.1002/2015JA021888](https://agupubs.onlinelibrary.wiley.com/doi/abs/10.1002/2015JA021888) (eprint:

- 411 <https://agupubs.onlinelibrary.wiley.com/doi/pdf/10.1002/2015JA021888> doi:  
412 10.1002/2015JA021888
- 413 Dunn, W. R., Gray, R., Wibisono, A. D., Lamy, L., Louis, C., Badman,  
414 S. V., ... Kraft, R. (2020). Comparisons Between Jupiter's X-ray,  
415 UV and Radio Emissions and In-Situ Solar Wind Measurements Dur-  
416 ing 2007. *Journal of Geophysical Research: Space Physics*, 125(6),  
417 e2019JA027222. Retrieved 2020-07-13, from [https://agupubs](https://agupubs.onlinelibrary.wiley.com/doi/abs/10.1029/2019JA027222)  
418 [.onlinelibrary.wiley.com/doi/abs/10.1029/2019JA027222](https://agupubs.onlinelibrary.wiley.com/doi/abs/10.1029/2019JA027222) (eprint:  
419 <https://agupubs.onlinelibrary.wiley.com/doi/pdf/10.1029/2019JA027222>) doi:  
420 10.1029/2019JA027222
- 421 Elsner, R. F., Lugaz, N., Waite, J. H., Cravens, T. E., Gladstone, G. R., Ford,  
422 P., ... Majeed, T. (2005, January). Simultaneous Chandra X ray, Hubble  
423 Space Telescope ultraviolet, and Ulysses radio observations of Jupiter's aurora.  
424 *Journal of Geophysical Research: Space Physics*, 110(A1). Retrieved 2018-08-  
425 31, from [https://agupubs.onlinelibrary.wiley.com/doi/abs/10.1029/](https://agupubs.onlinelibrary.wiley.com/doi/abs/10.1029/2004JA010717)  
426 [2004JA010717](https://agupubs.onlinelibrary.wiley.com/doi/abs/10.1029/2004JA010717) doi: 10.1029/2004JA010717
- 427 Gladstone, G. R., Jr, J. H. W., Grodent, D., Lewis, W. S., Crary, F. J., Elsner,  
428 R. F., ... Cravens, T. E. (2002, February). A pulsating auroral X-ray hot  
429 spot on Jupiter. *Nature*, 415(6875), 1000–1003. Retrieved 2018-08-31, from  
430 <https://www.nature.com/articles/4151000a> doi: 10.1038/4151000a
- 431 Gladstone, G. R., Persyn, S. C., Eterno, J. S., Walther, B. C., Slater, D. C., Davis,  
432 M. W., ... Denis, F. (2017, November). The Ultraviolet Spectrograph on  
433 NASA's Juno Mission. *Space Science Reviews*, 213(1), 447–473. Retrieved  
434 2018-10-24, from <https://doi.org/10.1007/s11214-014-0040-z> doi:  
435 10.1007/s11214-014-0040-z
- 436 Greathouse, T. K., Gladstone, G. R., Davis, M. W., Slater, D. C., Versteeg, M. H.,  
437 Persson, K. B., ... Eterno, J. S. (2013, September). Performance results  
438 from in-flight commissioning of the Juno Ultraviolet Spectrograph (Juno-  
439 UVS). In *UV, X-Ray, and Gamma-Ray Space Instrumentation for Astronomy*  
440 *XVIII* (Vol. 8859, p. 88590T). International Society for Optics and Photon-  
441 ics. Retrieved 2018-09-10, from [https://www.spiedigitallibrary.org/](https://www.spiedigitallibrary.org/conference-proceedings-of-spie/8859/88590T/Performance-results-from-in-flight-commissioning-of-the-Juno-Ultraviolet/10.1117/12.2024537.short)  
442 [conference-proceedings-of-spie/8859/88590T/Performance-results](https://www.spiedigitallibrary.org/conference-proceedings-of-spie/8859/88590T/Performance-results-from-in-flight-commissioning-of-the-Juno-Ultraviolet/10.1117/12.2024537.short)  
443 [-from-in-flight-commissioning-of-the-Juno-Ultraviolet/10.1117/](https://www.spiedigitallibrary.org/conference-proceedings-of-spie/8859/88590T/Performance-results-from-in-flight-commissioning-of-the-Juno-Ultraviolet/10.1117/12.2024537.short)  
444 [12.2024537.short](https://www.spiedigitallibrary.org/conference-proceedings-of-spie/8859/88590T/Performance-results-from-in-flight-commissioning-of-the-Juno-Ultraviolet/10.1117/12.2024537.short) doi: 10.1117/12.2024537
- 445 Grodent, D., Bonfond, B., Gérard, J.-C., Radioti, A., Gustin, J., Clarke, J. T.,  
446 ... Connerney, J. E. P. (2008, September). Auroral evidence of a localized  
447 magnetic anomaly in Jupiter's northern hemisphere. *Journal of Geophys-  
448 ical Research: Space Physics*, 113(A9). Retrieved 2018-09-03, from [https://](https://agupubs.onlinelibrary.wiley.com/doi/abs/10.1029/2008JA013185)  
449 [agupubs.onlinelibrary.wiley.com/doi/abs/10.1029/2008JA013185](https://agupubs.onlinelibrary.wiley.com/doi/abs/10.1029/2008JA013185) doi:  
450 10.1029/2008JA013185
- 451 Grodent, D., Clarke, J. T., Waite, J. H., Cowley, S. W. H., Gérard, J.-C., & Kim,  
452 J. (2003, October). Jupiter's polar auroral emissions. *Journal of Geophysical*  
453 *Research: Space Physics*, 108(A10). Retrieved 2018-09-03, from [https://](https://agupubs.onlinelibrary.wiley.com/doi/abs/10.1029/2003JA010017)  
454 [agupubs.onlinelibrary.wiley.com/doi/abs/10.1029/2003JA010017](https://agupubs.onlinelibrary.wiley.com/doi/abs/10.1029/2003JA010017) doi:  
455 10.1029/2003JA010017
- 456 Gustin, J., Gérard, J. C., Grodent, D., Gladstone, G. R., Clarke, J. T., Pryor,  
457 W. R., ... Ajello, J. M. (2013, September). Effects of methane on giant  
458 planet's UV emissions and implications for the auroral characteristics. *Jour-  
459 nal of Molecular Spectroscopy*, 291, 108–117. Retrieved 2019-02-26, from  
460 <http://www.sciencedirect.com/science/article/pii/S0022285213000441>  
461 doi: 10.1016/j.jms.2013.03.010
- 462 Gérard, J.-C., Bonfond, B., Mauk, B. H., Gladstone, G. R., Yao, Z. H., Greathouse,  
463 T. K., ... Levin, S. M. (2019). Contemporaneous Observations of Jovian  
464 Energetic Auroral Electrons and Ultraviolet Emissions by the Juno Spacecraft.  
465 *Journal of Geophysical Research: Space Physics*, 124(11), 8298–8317. Re-

- 466        retrieved 2020-01-22, from [https://agupubs.onlinelibrary.wiley.com/doi/](https://agupubs.onlinelibrary.wiley.com/doi/abs/10.1029/2019JA026862)  
467        [abs/10.1029/2019JA026862](https://agupubs.onlinelibrary.wiley.com/doi/abs/10.1029/2019JA026862) doi: 10.1029/2019JA026862
- 468   Hue, V., Gladstone, G. R., Greathouse, T. K., Kammer, J. A., Davis, M. W., Bon-  
469   fond, B., ... Byron, B. D. (2019, February). In-flight Characterization and  
470   Calibration of the Juno-ultraviolet Spectrograph (Juno-UVS). *The Astro-*  
471   *nomical Journal*, 157(2), 90. Retrieved 2019-11-19, from [https://doi.org/](https://doi.org/10.3847/2F1538-3881/2Faafb36)  
472   [10.3847/2F1538-3881/2Faafb36](https://doi.org/10.3847/2F1538-3881/2Faafb36) doi: 10.3847/1538-3881/aafb36
- 473   Jackman, C. M., Knigge, C., Altamirano, D., Gladstone, R., Dunn, W., Elsner, R.,  
474   ... Ford, P. (2018). Assessing Quasi-Periodicities in Jovian X-Ray Emissions:  
475   Techniques and Heritage Survey. *Journal of Geophysical Research: Space*  
476   *Physics*, 123(11), 9204–9221. Retrieved 2020-05-18, from [https://agupubs](https://agupubs.onlinelibrary.wiley.com/doi/abs/10.1029/2018JA025490)  
477   [.onlinelibrary.wiley.com/doi/abs/10.1029/2018JA025490](https://agupubs.onlinelibrary.wiley.com/doi/abs/10.1029/2018JA025490) (.eprint:  
478   <https://agupubs.onlinelibrary.wiley.com/doi/pdf/10.1029/2018JA025490>) doi:  
479   10.1029/2018JA025490
- 480   MacDowall, R. J., Kaiser, M. L., Desch, M. D., Farrell, W. M., Hess, R. A., &  
481   Stone, R. G. (1993, November). Quasiperiodic Jovian Radio bursts: ob-  
482   servations from the Ulysses Radio and Plasma Wave Experiment. *Plan-*  
483   *etary and Space Science*, 41(11), 1059–1072. Retrieved 2020-01-23, from  
484   <http://www.sciencedirect.com/science/article/pii/003206339390109F>  
485   doi: 10.1016/0032-0633(93)90109-F
- 486   Manners, H., Masters, A., & Yates, J. N. (2018). Standing Alfvén Waves in  
487   Jupiter’s Magnetosphere as a Source of 10- to 60-Min Quasiperiodic Pul-  
488   sations. *Geophysical Research Letters*, 45(17), 8746–8754. Retrieved  
489   2019-06-07, from [https://agupubs.onlinelibrary.wiley.com/doi/abs/](https://agupubs.onlinelibrary.wiley.com/doi/abs/10.1029/2018GL078891)  
490   [10.1029/2018GL078891](https://agupubs.onlinelibrary.wiley.com/doi/abs/10.1029/2018GL078891) (tex.ids: mannersStandingAlfvenWaves2018a) doi:  
491   10.1029/2018GL078891
- 492   Mauk, B. H., Clarke, J. T., Grodent, D., Waite, J. H., Paranicas, C. P., & Williams,  
493   D. J. (2002). Transient aurora on Jupiter from injections of magnetospheric  
494   electrons. *Nature*, 415, 1003–1005.
- 495   McKibben, R. B., Simpson, J. A., & Zhang, M. (1993, November). Impul-  
496   sive bursts of relativistic electrons discovered during Ulysses’ traversal of  
497   Jupiter’s dusk-side magnetosphere. *Planet. Space Sci.*, 41, 1041–1058. doi:  
498   10.1016/0032-0633(93)90108-E
- 499   Nichols, J. D., Badman, S. V., Bagenal, F., Bolton, S. J., Bonfond, B., Bunce, E. J.,  
500   ... Yoshikawa, I. (2017). Response of Jupiter’s auroras to conditions in  
501   the interplanetary medium as measured by the Hubble Space Telescope and  
502   Juno. *Geophysical Research Letters*, 44(15), 7643–7652. Retrieved 2019-04-  
503   26, from [https://agupubs.onlinelibrary.wiley.com/doi/abs/10.1002/](https://agupubs.onlinelibrary.wiley.com/doi/abs/10.1002/2017GL073029)  
504   [2017GL073029](https://agupubs.onlinelibrary.wiley.com/doi/abs/10.1002/2017GL073029) doi: 10.1002/2017GL073029
- 505   Nichols, J. D., Clarke, J. T., Gérard, J. C., & Grodent, D. (2009). Observations of  
506   Jovian polar auroral filaments. *Geophys. Res. Lett.*, 36, 8101. doi: 10.1029/  
507   2009GL037578
- 508   Nichols, J. D., Yeoman, T. K., Bunce, E. J., Chowdhury, M. N., Cowley, S. W. H.,  
509   & Robinson, T. R. (2017). Periodic Emission Within Jupiter’s Main Auroral  
510   Oval. *Geophysical Research Letters*, 44(18), 9192–9198. Retrieved 2019-03-  
511   25, from [https://agupubs.onlinelibrary.wiley.com/doi/abs/10.1002/](https://agupubs.onlinelibrary.wiley.com/doi/abs/10.1002/2017GL074824)  
512   [2017GL074824](https://agupubs.onlinelibrary.wiley.com/doi/abs/10.1002/2017GL074824) doi: 10.1002/2017GL074824
- 513   Pallier, L., & Prangé, R. (2001, August). More about the structure of the high  
514   latitude Jovian aurorae. *Planetary and Space Science*, 49(10), 1159–1173. Re-  
515   trieved 2018-08-31, from [http://www.sciencedirect.com/science/article/](http://www.sciencedirect.com/science/article/pii/S003206330100023X)  
516   [pii/S003206330100023X](http://www.sciencedirect.com/science/article/pii/S003206330100023X) doi: 10.1016/S0032-0633(01)00023-X
- 517   Pryor, W. R., Stewart, A. I. F., Esposito, L. W., McClintock, W. E., Colwell, J. E.,  
518   Jouchoux, A. J., ... Dougherty, M. K. (2005, November). Cassini UVIS ob-  
519   servations of Jupiter’s auroral variability. *Icarus*, 178(2), 312–326. Retrieved  
520   2020-05-13, from <http://www.sciencedirect.com/science/article/pii/>

- 521 S0019103505002265 doi: 10.1016/j.icarus.2005.05.021  
 522 Swithenbank-Harris, B. G., Nichols, J. D., & Bunce, E. J. (2019). Jupiter’s  
 523 Dark Polar Region as Observed by the Hubble Space Telescope Dur-  
 524 ing the Juno Approach Phase. *Journal of Geophysical Research: Space*  
 525 *Physics*, 124(11), 9094–9105. Retrieved 2020-04-11, from [https://agupubs](https://agupubs.onlinelibrary.wiley.com/doi/abs/10.1029/2019JA027306)  
 526 [.onlinelibrary.wiley.com/doi/abs/10.1029/2019JA027306](https://agupubs.onlinelibrary.wiley.com/doi/abs/10.1029/2019JA027306) (\_eprint:  
 527 <https://agupubs.onlinelibrary.wiley.com/doi/pdf/10.1029/2019JA027306>) doi:  
 528 10.1029/2019JA027306
- 529 Vogt, M. F., Bunce, E. J., Kivelson, M. G., Khurana, K. K., Walker, R. J., Radioti,  
 530 A., ... Grodent, D. (2015, April). Magnetosphere-ionosphere mapping at  
 531 Jupiter: Quantifying the effects of using different internal field models. *Journal*  
 532 *of Geophysical Research: Space Physics*, 120(4), 2584–2599. Retrieved 2018-  
 533 08-30, from [https://agupubs.onlinelibrary.wiley.com/doi/abs/10.1002/](https://agupubs.onlinelibrary.wiley.com/doi/abs/10.1002/2014JA020729)  
 534 [2014JA020729](https://agupubs.onlinelibrary.wiley.com/doi/abs/10.1002/2014JA020729) doi: 10.1002/2014JA020729
- 535 Vogt, M. F., Kivelson, M. G., Khurana, K. K., Walker, R. J., Bonfond, B., Gro-  
 536 dent, D., & Radioti, A. (2011, March). Improved mapping of Jupiter’s  
 537 auroral features to magnetospheric sources. *Journal of Geophysical Re-*  
 538 *search: Space Physics*, 116(A3). Retrieved 2019-02-25, from [https://](https://agupubs.onlinelibrary.wiley.com/doi/full/10.1029/2010JA016148)  
 539 [agupubs.onlinelibrary.wiley.com/doi/full/10.1029/2010JA016148](https://agupubs.onlinelibrary.wiley.com/doi/full/10.1029/2010JA016148)  
 540 doi: 10.1029/2010JA016148
- 541 Waite, J. H., Gladstone, G. R., Lewis, W. S., Goldstein, R., McComas, D. J., Ri-  
 542 ley, P., ... Young, D. T. (2001). An auroral flare at Jupiter. *Nature*, 410,  
 543 787–789.
- 544 Weigt, D. M., Jackman, C. M., Dunn, W. R., Gladstone, G. R., Vogt,  
 545 M. F., Wibisono, A. D., ... Kraft, R. P. (2020). Chandra Ob-  
 546 servations of Jupiter’s X-ray Auroral Emission During Juno Apo-  
 547 jove 2017. *Journal of Geophysical Research: Planets*, 125(4),  
 548 e2019JE006262. Retrieved 2020-03-29, from [https://agupubs](https://agupubs.onlinelibrary.wiley.com/doi/abs/10.1029/2019JE006262)  
 549 [.onlinelibrary.wiley.com/doi/abs/10.1029/2019JE006262](https://agupubs.onlinelibrary.wiley.com/doi/abs/10.1029/2019JE006262) (\_eprint:  
 550 <https://agupubs.onlinelibrary.wiley.com/doi/pdf/10.1029/2019JE006262>) doi:  
 551 10.1029/2019JE006262
- 552 Wibisono, A. D., Branduardi-Raymont, G., Dunn, W. R., Coates, A. J., Weigt,  
 553 D. M., Jackman, C. M., ... Fleming, D. (2020). Temporal and Spec-  
 554 tral Studies by XMM-Newton of Jupiter’s X-ray Auroras During a  
 555 Compression Event. *Journal of Geophysical Research: Space Physics*,  
 556 125(5), e2019JA027676. Retrieved 2020-07-10, from [https://agupubs](https://agupubs.onlinelibrary.wiley.com/doi/abs/10.1029/2019JA027676)  
 557 [.onlinelibrary.wiley.com/doi/abs/10.1029/2019JA027676](https://agupubs.onlinelibrary.wiley.com/doi/abs/10.1029/2019JA027676) (\_eprint:  
 558 <https://agupubs.onlinelibrary.wiley.com/doi/pdf/10.1029/2019JA027676>) doi:  
 559 10.1029/2019JA027676
- 560 Zhang, B., Delamere, P. A., Yao, Z., Bonfond, B., Lin, D., Sorathia, K. A., ...  
 561 Lyon, J. G. (2020, June). How Jupiter’s Unusual Magnetospheric Topology  
 562 Structures Its Aurora. *arXiv e-prints*, 2006, arXiv:2006.14834. Retrieved  
 563 2020-07-10, from <http://adsabs.harvard.edu/abs/2020arXiv200614834Z>

# Supporting Information for ”Morphology of Jupiter’s Polar Auroral Bright Spot Emissions via Juno-UVS Observations”

K. Haewsantati<sup>1,2,3,4</sup>, B. Bonfond<sup>1</sup>, S. Wannawichian<sup>3,4</sup>, G. R. Gladstone<sup>5</sup>,  
V. Hue<sup>5</sup>, M. H. Versteeg<sup>5</sup>, T. K. Greathouse<sup>5</sup>, D. Grodent<sup>1</sup>, Z. Yao<sup>6,1</sup>, W.  
Dunn<sup>7,8,9</sup>, J.-C. Gérard<sup>1</sup>, R. Giles<sup>5</sup>, J. Kammer<sup>5</sup>, R. Guo<sup>1</sup>, M. F. Vogt<sup>10</sup>

<sup>1</sup>LPAP, STAR Institute, Université de Liège, Liège, Belgium

<sup>2</sup>Ph.D. program in Physics, Department of Physics and Materials Science, Faculty of Science, Chiang Mai University, Chiang Mai,

Thailand

<sup>3</sup>Department of Physics and Materials Science, Faculty of Science, Chiang Mai University, Chiang Mai, Thailand

<sup>4</sup>National Astronomical Research Institute of Thailand (Public Organization), Chiang Mai, Thailand

<sup>5</sup>Southwest Research Institute, San Antonio, Texas, USA

<sup>6</sup>Key Laboratory of Earth and Planetary Physics, Institute of Geology and Geophysics, Chinese Academy of Sciences, Beijing, China

<sup>7</sup>Mullard Space Science Laboratory, Department of Space and Climate Physics, University College London, Dorking, UK

<sup>8</sup>The Centre for Planetary Science at UCL/Birkbeck, London, UK

<sup>9</sup>Harvard-Smithsonian Center for Astrophysics, Smithsonian Astrophysical Observatory, Cambridge, MA USA

<sup>10</sup>Center for Space Physics, Boston University, Boston, MA, USA

## Contents of this file

1. Figures S1 to S5

## Additional Supporting Information (Files uploaded separately)

---

1. Captions for large Table S1

## Introduction

The supporting information materials are following.

1. The histogram shows the distribution of the solar zenith angles of bright spots which represent the relation between the bright spot occurrence and the exposure to the sunlight.
2. We show the polar projection of bright spots and the SIII longitude position after extrapolation to location that can be mapped by Vogt's mapping model.
3. The color ratio plot shows bright spot detected during PJ1 in high color ratio region.
4. We also show the power variation for PJ4 which has quasiperiodic behaviors as same as the PJ16 power variation plot (Figure 6.)
5. Based on period analysis using Lomb-Scargle periodogram method for bright spots during PJ4 and PJ16, the Lomb Normalized Periodogram will be presented.

## References

- Bonfond, B., Gladstone, G. R., Grodent, D., Greathouse, T. K., Versteeg, M. H., Hue, V., ... Kurth, W. S. (2017, May). Morphology of the UV aurorae Jupiter during Juno's first perijove observations. *Geophysical Research Letters*, *44*(10), 4463–4471. Retrieved 2019-02-25, from <https://agupubs.onlinelibrary.wiley.com/doi/full/10.1002/2017GL073114> doi: 10.1002/2017GL073114
- Bonfond, B., Saur, J., Grodent, D., Badman, S. V., Bisikalo, D., Shematovich, V., ... Radioti, A. (2017, August). The tails of the satellite auroral footprints at Jupiter. *Journal of Geophysical Research: Space Physics*, *122*(8), 7985–7996. Retrieved 2018-08-31, from <https://agupubs.onlinelibrary.wiley.com/doi/abs/>

10.1002/2017JA024370 doi: 10.1002/2017JA024370

Connerney, J. E. P., Kotsiaros, S., Oliverson, R. J., Espley, J. R., Joergensen, J. L., Joergensen, P. S., ... Levin, S. M. (2018, March). A New Model of Jupiter's Magnetic Field From Juno's First Nine Orbits. *Geophysical Research Letters*, 45(6), 2590–2596. Retrieved 2018-10-25, from <https://agupubs.onlinelibrary.wiley.com/doi/abs/10.1002/2018GL077312> doi: 10.1002/2018GL077312

Vogt, M. F., Bunce, E. J., Kivelson, M. G., Khurana, K. K., Walker, R. J., Radioti, A., ... Grodent, D. (2015, April). Magnetosphere-ionosphere mapping at Jupiter: Quantifying the effects of using different internal field models. *Journal of Geophysical Research: Space Physics*, 120(4), 2584–2599. Retrieved 2018-08-30, from <https://agupubs.onlinelibrary.wiley.com/doi/abs/10.1002/2014JA020729> doi: 10.1002/2014JA020729

Vogt, M. F., Kivelson, M. G., Khurana, K. K., Walker, R. J., Bonfond, B., Grodent, D., & Radioti, A. (2011, March). Improved mapping of Jupiter's auroral features to magnetospheric sources. *Journal of Geophysical Research: Space Physics*, 116(A3). Retrieved 2019-02-25, from <https://agupubs.onlinelibrary.wiley.com/doi/full/10.1029/2010JA016148> doi: 10.1029/2010JA016148

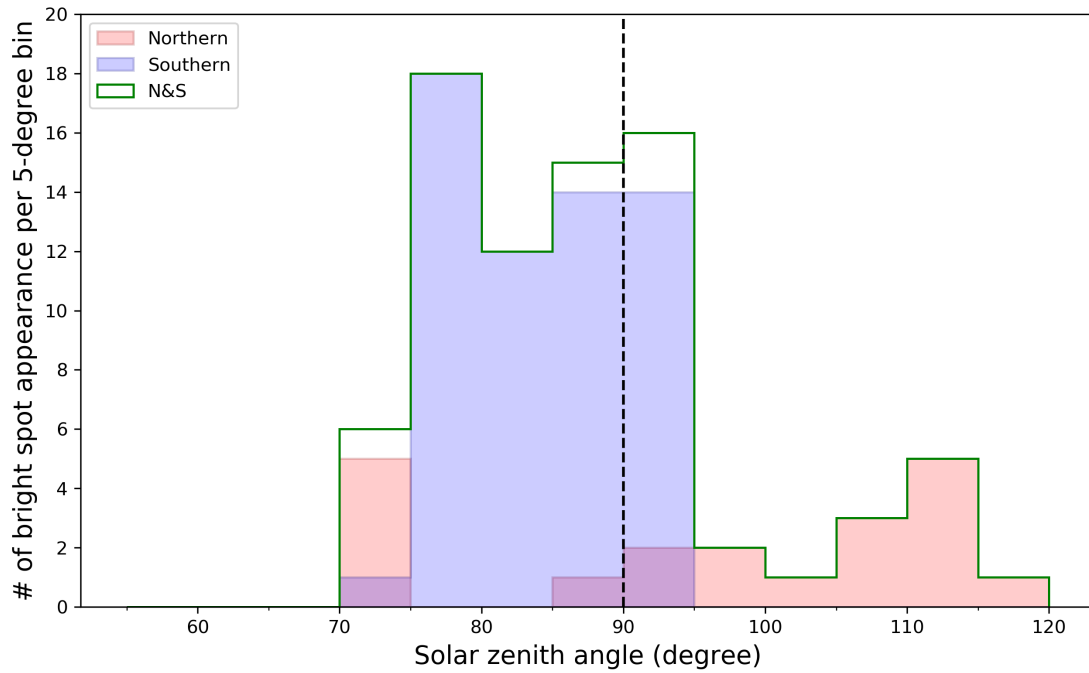


**Figure S1.** Distribution of solar zenith angles of bright spots in Northern hemisphere (pink), Southern hemisphere (blue), and the combined spots from both hemispheres (green line). The dashed vertical line represents  $90^\circ$  zenith angle at which the sun is on the horizon. The angles larger than  $90^\circ$  refer to the case that the sun is below the horizon, corresponding to the night time.

**Table S1.** The bright spot characteristics observed during PJ1 to PJ25 are presented. The power is calculated from the total brightness in bright spot's elliptical area. This power is different from the power variation plot (Figure 6 and Figure S4) which is the integrated area corresponding to all bright spots detected during a perijove. The last two columns are mapped positions in magnetosphere and the local times from Vogt's magnetic flux equivalent using JRM09 model.

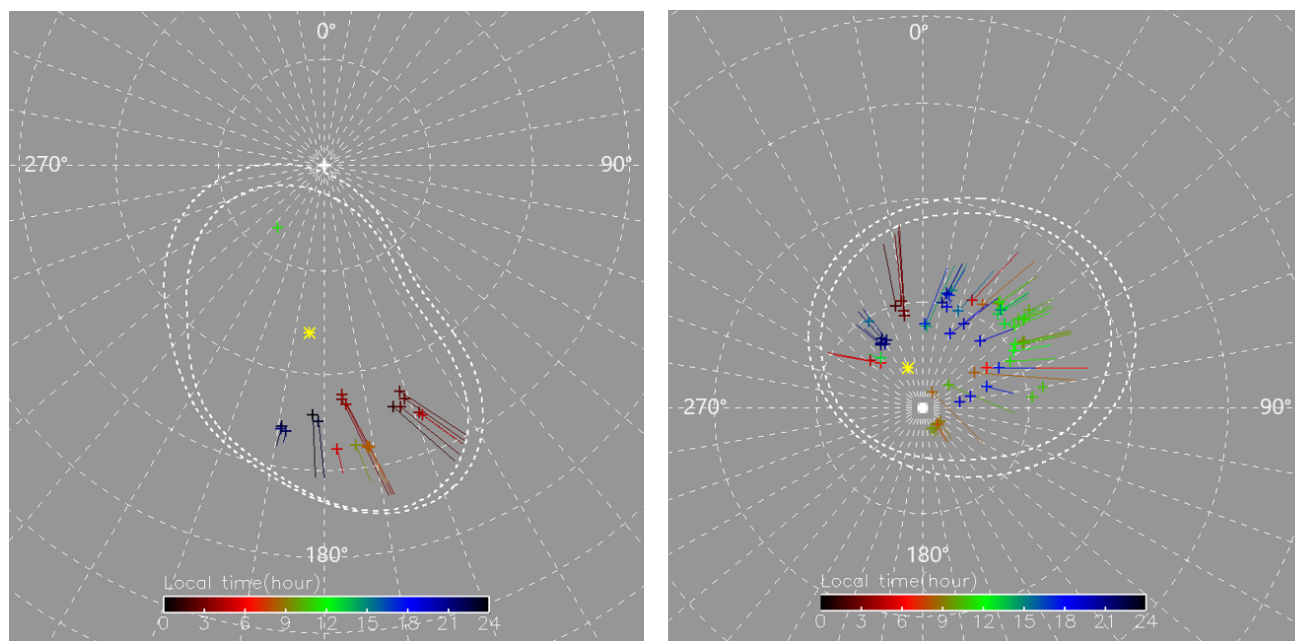


**Figure S2.** Polar projections (Left: Northern, right: Southern) show positions of bright spots and local times according to Vogt's magnetic flux equivalent mapping with JRM09 model. The grid represents meridians and parallels in the SIII jovi-centric system, spaced every  $10^\circ$ . The two dash contours are the statistical locations of the main emission for the compressed and expanded cases (Bonfond, Gladstone, et al., 2017). The yellow asterisk represents the magnetic pole of each hemisphere (Bonfond, Saur, et al., 2017; Connerney et al., 2018). The lines represent the tracing paths from the magnetic pole to the bright spots' peak positions in the directions toward system III longitudes and latitudes, which can be mapped by Vogt's mapping model. (Vogt et al., 2011, 2015)

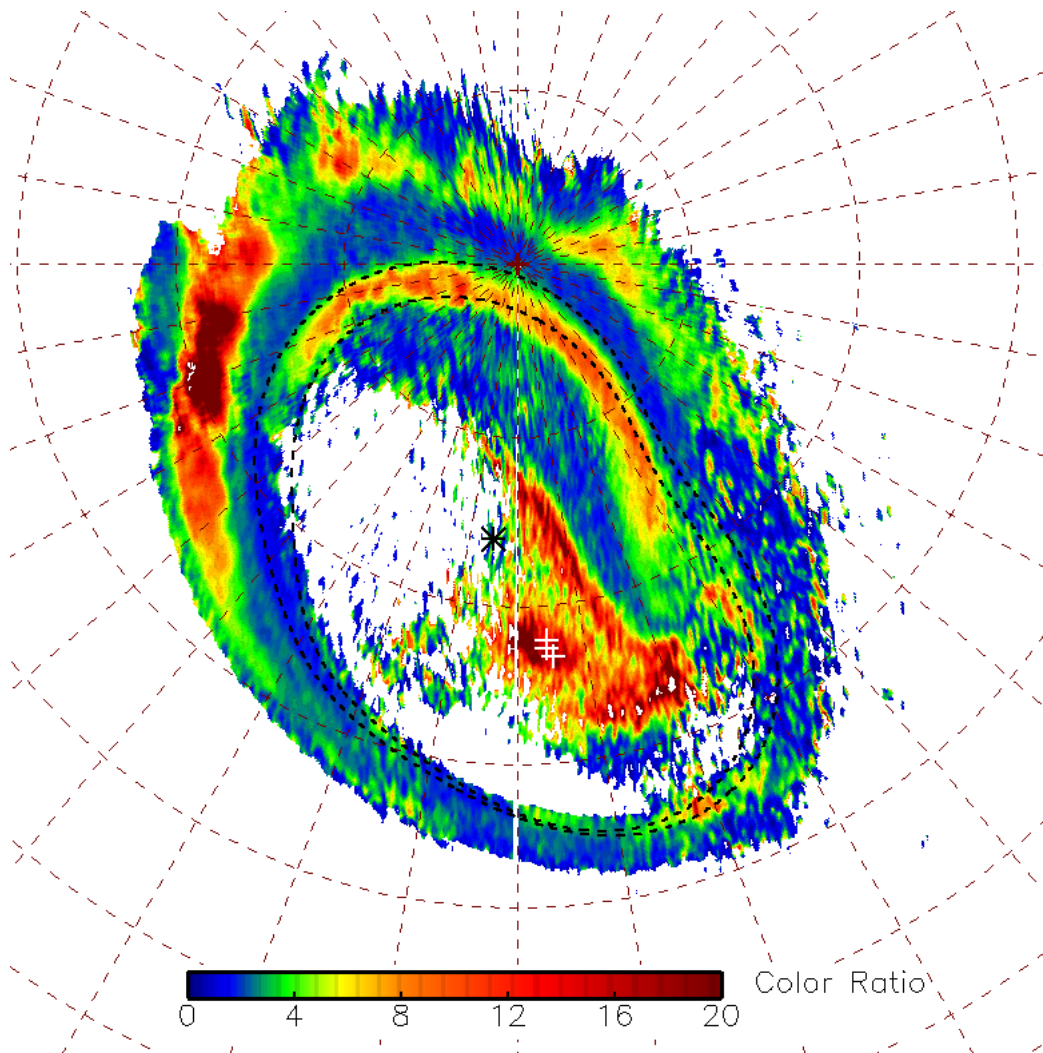


**Figure S3.** The color ratio map observed from PJ1 shows the bright spots positions (plus symbols) in high color ratio region. The asterisk represents the magnetic pole. The grid coordinates and two dashed contours are the same as in figure S2.

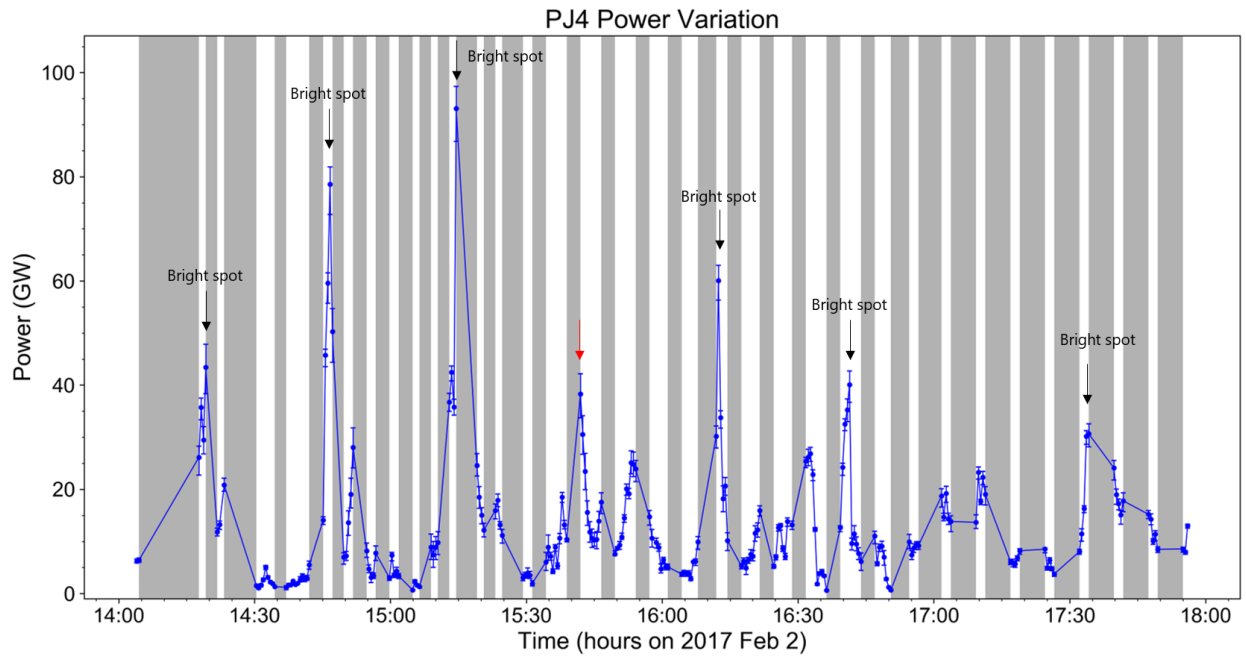


**Figure S4.** The power variation as a function of time for the southern bright spots during PJ4. The black arrows indicate the times that bright spots appear in UVS view. The red arrow presents the peak at which no bright spot appears but there is the increase in the brightness in the region of interest. The grey areas indicate times when the region of interest is covered by UVS view less than 50%.

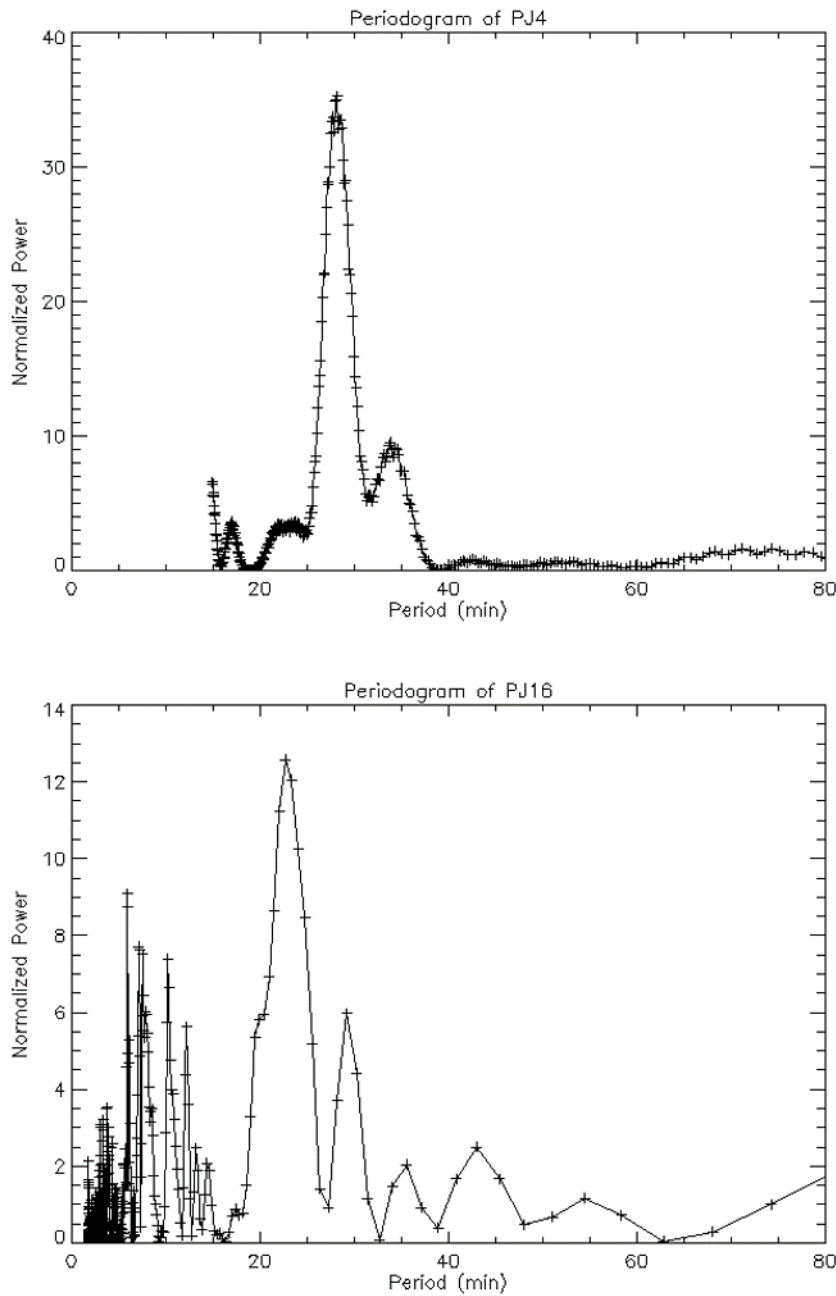


**Figure S5.** Fitted result from Lomb-Scargle periodogram for PJ4 (top) and PJ16 (bottom). The dashed lines represent significant levels. The lower significant level implies the high probability for the period to be important. The highest peak of normalized power for PJ4 corresponds to period 28.18 minutes. In addition, for PJ16, the clearest peak of normalized power in our period range is 22.68 minutes.

**Table S1.** Bright spot characteristics

PJ	Date	Time	Peak's position		Power (GW)	Surface area ( $\times 10^6$ km <sup>2</sup> )	Magnetic flux ( $\times 10^9$ Wb)	Ionospheric local time	Vogt's mapping result	
			Latitude	Longitude					Position ( $R_J$ )	Local time (h)
PJ1	8/27/2016	10:00:01	67.3489	175.632	103.133	9.156	5580.420	7.116	143.393	2.84056
PJ1	8/27/2016	10:15:53	67.8432	175.539	68.922	10.477	6429.260	7.873	141.845	3.42373
PJ1	8/27/2016	10:19:28	66.8182	174.753	56.162	7.997	4823.740	7.972	141.502	3.70408
PJ3	12/11/2016	14:56:59	65.6758	164.029	39.371	4.102	2881.550	3.840	149.348	1.21778
PJ3	12/11/2016	15:01:32	66.9921	161.503	88.089	9.643	6839.500	4.589	146.267	2.29083
PJ3	12/11/2016	15:13:10	66.1218	160.968	78.691	8.134	5817.300	4.943	149.452	2.42041
PJ3	12/11/2016	15:21:15	65.458	162.437	23.956	2.967	2113.490	4.976	148.021	2.27462
PJ3	12/11/2016	15:42:27	64.2582	158.95	81.811	7.685	5722.400	6.038	143.476	3.34408
PJ3	12/11/2016	16:12:17	63.8974	158.489	14.468	1.364	1055.040	7.239	135.893	4.46139
PJ3	12/11/2016	14:45:21	64.0401	189.29	26.241	5.842	2799.420	23.034	131.527	20.7002
PJ3	12/11/2016	15:18:43	63.8654	188.179	56.005	5.051	2409.250	0.581	144.07	21.8748
PJ3	12/11/2016	15:52:34	64.3051	189.202	21.741	1.220	579.654	1.746	147.002	22.8547
PJ4	2/2/2017	14:18:13	-78.5853	14.0362	21.510	1.746	1926.980	12.695	92.0647	14.417
PJ4	2/2/2017	14:46:10	-78.9183	12.0115	54.170	5.377	5851.510	13.959	99.8606	15.9231
PJ4	2/2/2017	15:14:32	-79.0946	13.4486	89.820	9.207	10244.600	14.951	107.664	16.968
PJ4	2/2/2017	16:12:25	-80.2062	13.6005	50.826	5.617	6280.220	17.097	148.886	19.0696
PJ4	2/2/2017	16:40:22	-78.9944	12.0947	30.718	7.850	8758.550	18.544	149.374	19.8545
PJ4	2/2/2017	17:33:40	-79.9242	10.5392	29.904	8.175	9180.190	20.699	147.419	20.9001
PJ6	5/19/2017	03:51:39	62.1384	170.806	94.076	6.634	4229.370	10.531	102.831	8.03681
PJ6	5/19/2017	03:52:40	62.2641	171.266	71.978	6.519	4252.650	10.518	101.114	8.13232
PJ6	5/19/2017	03:54:11	62.0802	171.155	82.254	10.248	6869.470	10.579	99.3184	8.23206
PJ6	5/19/2017	04:08:49	62.2366	177.375	70.110	7.534	4405.250	10.257	148.593	5.13488
PJ6	5/19/2017	04:22:26	62.5093	173.532	60.703	8.077	5242.050	11.410	89.5063	9.26073
PJ8	9/1/2017	20:47:45	82.6612	216.511	2.594	0.445	320.956	11.965	73.5976	11.2746
PJ8	9/1/2017	22:42:39	-83.0653	329.47	3.312	0.350	423.032	18.407	149.99	20.3766
PJ8	9/1/2017	23:17:50	-82.7975	327.155	2.187	0.464	561.052	20.074	149.512	21.1154

PJ8	9/1/2017	23:30:55	-82.9264	326.482	10.164	1.576	1904.370	20.732	148.272	21.5613
PJ8	9/1/2017	23:46:30	-82.8045	332.071	9.689	1.719	2077.170	20.541	149.824	21.5275
PJ8	9/1/2017	23:56:04	-82.4445	329.534	7.907	1.782	2151.990	21.208	148.143	21.6553
PJ9	10/24/2017	20:58:31	-76.298	47.5094	34.796	4.385	5103.280	10.602	90.9659	10.0248
PJ9	10/24/2017	21:11:08	-77.6322	47.2704	49.057	9.472	11143.500	10.999	92.4111	10.4482
PJ9	10/24/2017	21:13:09	-77.1139	48.8785	29.783	5.557	6564.570	11.023	91.7053	10.5553
PJ9	10/24/2017	21:25:47	-77.3349	48.9452	109.941	14.299	16969.000	11.506	92.2943	11.0453
PJ9	10/24/2017	21:32:21	-78.3933	48.4926	34.513	4.490	5383.320	11.685	89.6168	11.2084
PJ9	10/24/2017	21:53:33	-78.9105	44.4383	48.733	7.516	9097.410	12.748	89.7743	12.8518
PJ9	10/24/2017	22:29:23	-79.8573	57.9946	98.037	13.737	17469.000	13.176	88.6372	12.0939
PJ9	10/24/2017	22:30:54	-80.6291	62.1759	146.325	20.701	26725.600	12.868	86.547	11.3414
PJ12	4/1/2018	10:59:35	-83.387	312.184	24.804	1.881	2291.500	6.902	137.352	4.34857
PJ12	4/1/2018	11:20:34	-84.2603	317.161	12.506	1.327	1703.070	7.799	122.933	5.83077
PJ12	4/1/2018	11:13:24	-81.1704	348.983	7.340	0.985	1119.500	2.435	79.4951	2.48828
PJ12	4/1/2018	11:18:31	-80.074	345.211	8.953	1.569	1736.150	3.147	147.444	1.71082
PJ12	4/1/2018	11:54:48	-79.7424	348.774	13.536	2.562	2768.200	4.236	132.883	2.79601
PJ12	4/1/2018	11:56:20	-80.7	349.061	41.316	3.887	4399.730	4.199	123.593	2.87237
PJ13	5/24/2018	04:22:10	65.1589	181.273	19.209	1.507	846.061	1.631	136.407	23.023
PJ13	5/24/2018	04:47:31	65.8103	182.611	17.498	1.549	867.602	2.420	136.157	23.6283
PJ14	7/16/2018	06:31:39	-87.8921	136.469	20.000	2.217	3252.040	11.966	97.5102	8.22648
PJ14	7/16/2018	06:33:39	-87.8866	139.399	30.891	2.884	4193.630	11.981	99.6099	7.96567
PJ14	7/16/2018	06:38:10	-87.8755	127.694	28.599	2.285	3338.340	12.430	93.1937	8.77023
PJ14	7/16/2018	06:55:12	-87.7722	149.036	8.764	1.031	1472.670	12.637	92.0644	9.15722
PJ14	7/16/2018	07:01:43	-87.8428	157.068	14.951	1.370	1958.270	12.707	86.5823	9.60095
PJ15	9/7/2018	02:28:55	-82.8799	58.1906	6.461	0.722	989.899	12.707	115.911	6.33337
PJ15	9/7/2018	03:02:29	-84.0993	56.1038	3.704	1.290	1763.750	10.998	94.4549	8.18897
PJ15	9/7/2018	04:33:42	-86.7499	48.8141	14.053	3.326	4669.580	13.434	90.586	10.3344
PJ15	9/7/2018	04:37:12	-88.283	32.2756	43.550	4.959	7211.750	12.094	93.0438	8.39585
PJ16	10/29/2018	23:00:33	-78.8204	24.8027	51.881	3.709	4241.330	8.240	148.995	4.94903
PJ16	10/29/2018	23:29:09	-78.6979	30.2284	31.638	4.645	5312.320	8.985	97.0588	8.13252

PJ16	10/29/2018	23:56:15	-77.8215	36.0007	18.909	3.266	3759.260	9.753	94.48	9.40275
PJ16	10/30/2018	00:26:21	-77.6031	36.1582	41.142	5.927	6749.550	10.979	87.0123	11.2907
PJ16	10/30/2018	00:48:26	-77.9568	38.7742	31.673	6.176	7216.400	11.639	90.4642	12.0096
PJ16	10/30/2018	01:29:05	-78.6268	38.9623	81.816	9.845	11463.300	13.180	91.1544	13.2555
PJ16	10/30/2018	01:52:04	-78.1764	38.6598	157.713	12.770	15025.000	14.185	94.0923	14.9941
PJ20	5/29/2019	09:08:12	-78.5023	56.7351	13.048	1.653	2089.040	10.929	94.2201	9.49789
PJ20	5/29/2019	09:11:46	-78.7181	56.9598	9.032	0.713	898.851	11.033	92.2378	9.61732
PJ20	5/29/2019	09:14:18	-78.6289	57.7071	19.086	1.707	2147.060	11.099	90.1268	9.67043
PJ20	5/29/2019	09:49:22	-79.387	55.6197	3.359	0.976	1220.710	12.548	88.5162	11.6019
PJ21	7/21/2019	05:17:40	-80.4162	328.092	7.064	0.636	719.276	13.056	96.7069	15.6174
PJ21	7/21/2019	06:59:00	-82.3281	2.86245	24.467	4.432	5438.680	12.848	92.2783	14.3567
PJ21	7/21/2019	07:46:09	-82.1031	1.66836	63.929	7.726	9279.190	14.950	107.442	17.0867
PJ21	7/21/2019	08:00:12	-80.2607	20.2918	69.460	9.043	10553.700	14.164	97.7403	15.6688
PJ22	9/12/2019	07:34:24	-78.4555	80.4122	144.630	17.417	22926.200	12.953	89.7742	10.5494
PJ22	9/12/2019	07:50:56	-79.5817	84.4996	124.978	14.869	19931.700	13.285	89.5918	10.6388
PJ23	11/4/2019	00:31:30	-85.3625	76.6513	32.664	2.363	3321.070	22.436	132.311	18.6968
PJ23	11/4/2019	01:06:41	-86.4431	81.3475	25.556	2.010	2924.850	23.265	136.222	19.2979
PJ23	11/4/2019	01:01:09	-83.9144	320.102	23.796	4.261	5293.730	11.929	91.2448	13.1339
PJ24	12/26/2019	19:20:32	-82.5578	20.487	19.534	2.043	2559.610	17.734	148.054	19.0153
PJ24	12/26/2019	20:00:32	-81.1849	26.3421	79.836	6.799	8310.690	19.287	149.448	19.7707
PJ24	12/26/2019	20:44:34	-81.6846	40.8878	17.765	2.700	3415.000	19.882	149.648	19.0486
PJ24	12/26/2019	20:49:38	-81.8746	62.468	20.984	5.386	7294.450	19.882	115.385	17.4216
PJ24	12/26/2019	21:33:40	-83.6333	71.7829	86.355	6.293	9185.660	19.615	114.031	17.4712